# LESSONS LEARNED FROM CIRFT TESTING ON SNF VIBRATION INTEGRITY STUDY

J.-A. Wang, H. Wang, H. Jiang, B. Bevard, R. Howard, J. Scaglione
*Oak Ridge National Laboratory, One Bethel Valley Road, Oak Ridge, TN 37831*

A cyclic integrated reversible-bending fatigue tester (CIRFT) was developed to support U.S. NRC and DOE Used Fuel Disposition Campaign studies on high burn-up (HBU) spent nuclear fuel (SNF) transportation during normal conditions of transport (NCT). Two devices were developed; the first CIRFT was successfully installed and operated in the ORNL hot-cells in September 2013. Since hot cell testing commenced several HBU SNF samples from both Zr-4 and M5 clads were investigated. The second CIRFT device was developed in February 2014, and has been used to test clad/fuel surrogate rods (stainless steel with alumina pellet inserts). The second CIRFT machine has also been used for sensor development and test sensitivity analyses, as well as loading boundary condition parameter studies. The lessons learned from CIRFT testing will be presented in this paper.

## I. INTRODUCTION

The objective of this project is to perform a systematic study of SNF integrity under simulated transportation environments (normal conditions of transport [NCT]) using hot-cell testing technology developed at the Oak Ridge National Laboratory (ORNL)—the Cyclic Integrated Reversible-Bending Fatigue Tester (CIRFT) [Ref. 1–8]. Currently, the CIRFT testing on UNF is conducted at an ORNL hot-cell testing facility.

Under Nuclear Regulatory Commission (NRC) sponsorship, ORNL completed four benchmark tests, four static tests, and twelve dynamic or cycle tests on H. B. Robinson (HBR) high burn-up (HBU) fuel. The clad of the HBR fuel was made of Zircalloy-4. The related testing results will be documented in an NRC regulatory guide contractor-prepared (NUREG/CR) report. With support from the US Department of Energy (DOE), the CIRFT work has continued on remaining HBR rods. The CIRFT testing on North Anna (NA) M5 ™and mixed oxide (MOX) M5™ UNF were also initiated in the reporting period. At the same time, ORNL conducted post-irradiation examination (PIE) of selected HBR rod segment/tested specimens, along with fractography on tested NA M5™ and MOX fuels.

While the use of CIRFT on HBR UNF rods generated a lot of interesting data, a number of important issues remain to be addressed. Because direct examination of some of these issues in a hot cell is prohibitive due to high cost and limited access, out-of-cell study has been demonstrated to be cost effective and much more feasible. A testing system with the same configuration as that of CIRFT used in a hot cell has been developed to study the issues that emerged from hot-cell testing and also to investigate the fatigue and failure mechanisms of UNF rods that cannot be identified directly in hot-cell testing.

The development of hardware and software, CIRFT test results on HBR fuel rods, NA M5™ fuel rods, and

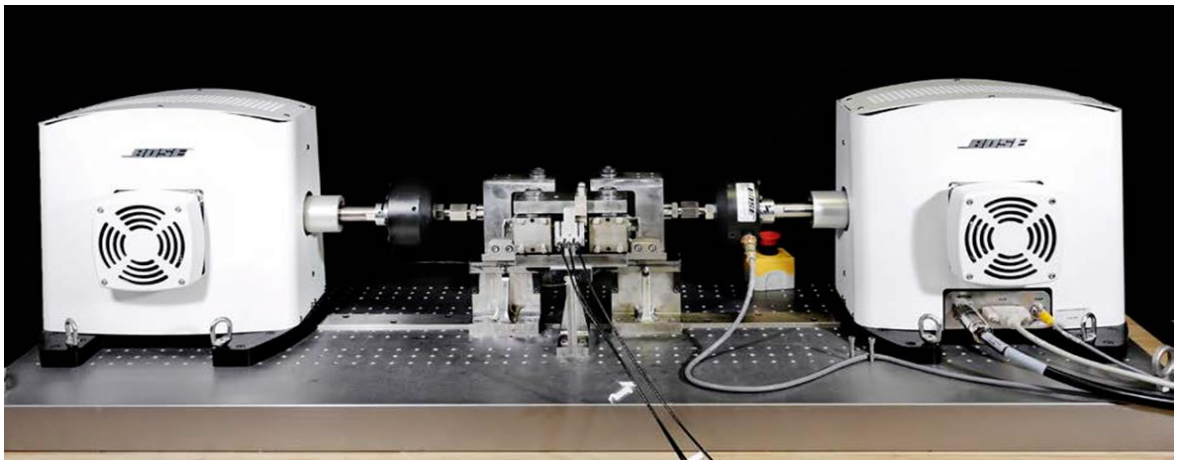

Fig. 1 Cyclic integrated reversible-bending fatigue tester, where the SNF is loaded in the central U-bent fixture

MOX fuel rods will be discussed in this report.

The information resulting from these studies, such as fuel contribution to clad stiffness, potential hydrogen effect, and pellet-clad interaction and their associated bonding efficiency effects, will be presented:

## II. CIRFT TESTING RESULTS OF H. B. ROBINSON USED FUEL

Under DOE sponsorship, ORNL conducted the CIRFT tests on rod specimens R3, R4 and R5 and conducted limited PIE. Brief descriptions of these tests and the PIE are given below. For detailed information on the testing system, the data processing method, and test results on other rod specimens based on HBR UNF [Ref. 5].

### II.A. Data Processing

Measurement data and online monitoring data were converted into applied moment and curvature based on the load channel output (load 1 and load 2), the loading arm (101.60 mm), and LVDT channels (LVDT 1, 2, and 3) output. The moment ($M$) was estimated by:

$$M = F \times L \quad \textbf{(1)}$$

where $F$ is the averaged value of applied loads (load 1 and load 2) from Bose dual motors, and $L$ is the loading arm, 101.60 mm. The curvature ($\kappa$) was estimated using Eq. (2) as described below.

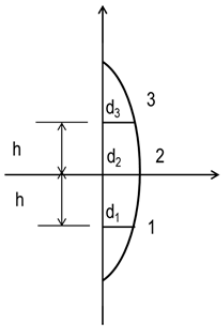


**The curvature κ can be defined by the radius of circle as follows**

$$\kappa = 1/R \quad \textbf{(2)}$$

**The parameters of circle equation can be estimated based on the deflections measured by three LVDTs, $d_1$, $d_2$, $d_3$:**

$$R = \sqrt{(x_0 - d_2)^2 + y_0^2}$$

$$x_0 = \frac{-2m_a m_b h - m_a(d_2 + d_3) + m_b(d_1 + d_2)}{2(m_b - m_a)}$$

$$y_0 = -\frac{1}{m_a}\left(x_0 - \frac{d_1 + d_2}{2}\right) - \frac{h}{2}$$

**where**

$$m_a = \frac{h}{d_2 - d_1} \qquad m_b = \frac{h}{d_3 - d_2}$$

The equivalent strain-stress curves were obtained under the assumption that the UNF rod can be idealized as a linear elastic homogeneous material without the consideration of the effects induced by any pellet-cladding interaction. The equivalent stress was calculated by:

$$\sigma = M \times y_{max}/I \quad \textbf{(3)}$$

where I is the moment of inertia, $I = I_c + I_p$, and $I_c$ and $I_p$ are moments of inertia of the cladding and pellet, respectively, and $y_{max}$ is the maximum distance to the neutral axis of the test rod of the section measured by the radius of the cladding. The calculation of stress disregards the difference of elastic moduli between the cladding and the pellets.

The equivalent strain was calculated by:

$$\varepsilon = \kappa \times y_{max}. \quad \textbf{(4)}$$

and flexural rigidity is defined as $\Delta M/\Delta\kappa$.

### II.B. Dynamic Testing Results

*II.B.1. D13/R3/606B3E under ±13.72 N·m 5 Hz*

The cycle test on sample D13/R3 (606B3E, 66.5 GWd/MTU burnup, 100–110 μm oxide layer, 750 ppm hydrogen content) was conducted under ±13.72 N·m at 5 Hz. Rod specimen R3 failed at approximately $1.29 \times 10^5$ cycles within the gauge section. Online monitoring showed that rigidity increased prior to the final rigidity drop at failure as shown in Fig. 2. The peak and valley of curvature data reflect the significant variation in curvature from the tension and compression side clad as seen by the drop in the peak value shown in Fig. 2d.

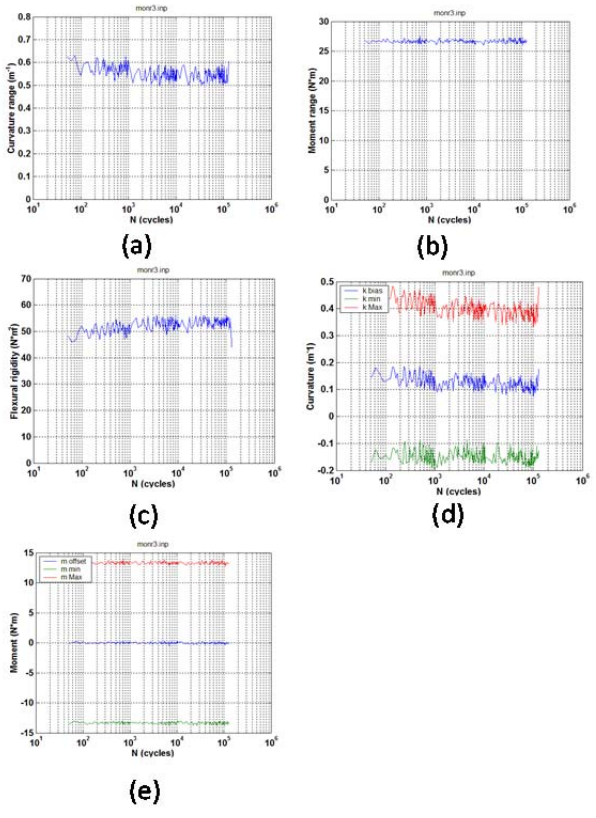


Fig. 2. Variations of (a) curvature range, (b) applied moment range, (c) flexural rigidity, (d) maximum and minimum values of curvature, and (e) maximum and minimum values of moment as a function of number of cycles for D13/R3 (606B3E); $N_f = 1.29 \times 10^5$ cycles under ±13.72 N·m 5 Hz.

The non-symmetry waveform change in peak and valley curvature measurement during the cyclic test are attributed to pellet-clad interaction, while under clad compression cycle the pellet-pellet pining can provide sufficient bending moment resistance, thus, reduces its curvature reading, and the additional reinforcement from pellet-pellet interaction would be diminished under clad tension cycle. The decreased rigidity was observed in the periodical quasi-static measurements, as shown in Fig. 3.

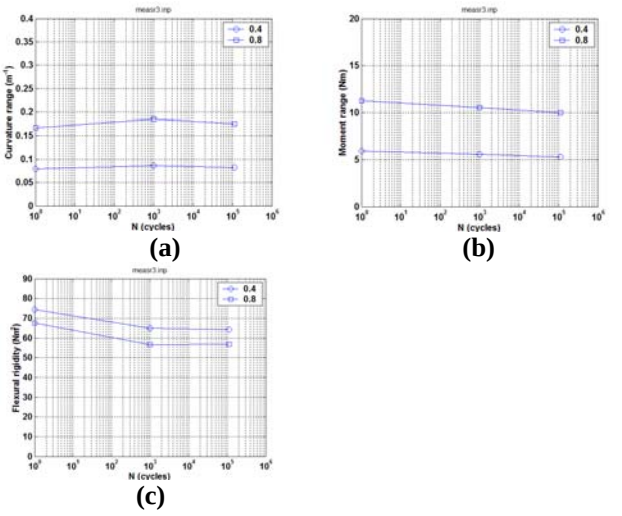


Fig. 3. Variations of (a) curvature range, (b) applied moment range, and (c) flexural rigidity as a function of number of cycles for D13/R3 (606B3E); $N_f = 1.29\times10^5$ cycles under ±13.72 N·m 5 Hz.

### II.C. Mean Curvature and Maximum of Absolute Curvature Extremes

Under a load-controlling mode, the offset of the M-κ loop with respect to the κ axis can be described by the mean value of curvatures, $\kappa_m$:

$$\kappa_m = 0.5 \times (\kappa_{max} + \kappa_{min}). \quad (5)$$

In load-controlled cycle tests, the curvature range $\Delta\kappa = (\kappa_{max} - \kappa_{min})$ exhibited a flat response prior to failure. As a result, the rigidity was stable over most of the monitored period, followed by a slight drop prior to failure. However, using curvature range/amplitude to characterize fatigue in UNF can be risky. This is because the response of rods is generally not symmetric with respect to the curvature origin, as seen in Fig. 2d. The sign and magnitude of the mean curvature depends on the as-received condition of a rod and on loading conditions. These observations raised a concern because the use of curvature range/amplitude did not reflect the real maximum stress level of the outer fiber in a bending rod.

An alternate approach is based on the maximum of absolute curvature extremes, $|\kappa|_{max}$, as defined by the following:

$$|k|_{max} = \max(|k_{max}|, |k_{min}|). \quad (6)$$

For a given specimen, the $|\kappa|_{max}$ given by Eq. (6) corresponds to the curvature that causes the maximum stress levels.

Curvature as a function of the number of cycles is shown in Fig. 4 in terms of both curvature amplitude and maximum of absolute curvature extremes. The results indicate that the curve of curvature versus the number of cycles could be raised to a certain degree if the maxima were used instead of amplitude. The factor of the power function was increased by 23%.

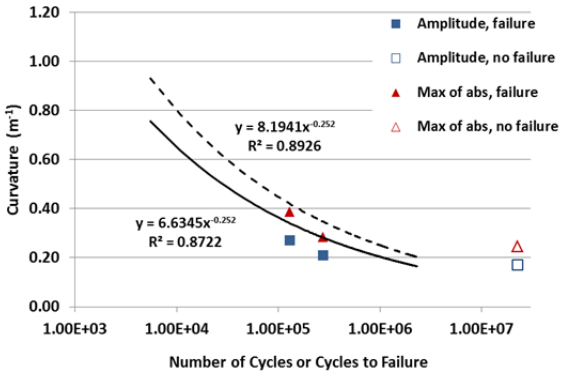


Fig. 4. Maxima of absolute (abs) curvature extremes and curvature amplitudes as a function of number of cycles. Solid markers represent tests with specimen failures; open markers indicate tests without failures. The power function was obtained from curve fitting based on the HBR data set [5]; solid line corresponds to amplitudes, and dash line corresponds to maxima of absolute.

### II.D. κ-N Curve and Effect of Hydrogen Contents

There was no specific hydrogen content data available for the tested HBR rod segments. However, the ranges of hydrogen content on the parent fuel rods were available, and the hydrogen contents of the tested rod segments can be estimated based on where they were taken. The estimated hydrogen contents of the HBR rods ranged from 360 to 750 ppm. An assembly of cycle tests is presented in Fig.5, with focus on the tests in which specimens failed. It can be clearly seen that the curve of curvature range vs. the number of cycles was shifted down and to the left when hydrogen content was equal to or greater than 700 ppm. Under the same curvature range, the fatigue life of the specimens with higher hydrogen content is shorter than the fatigue life of specimens with lower hydrogen content.

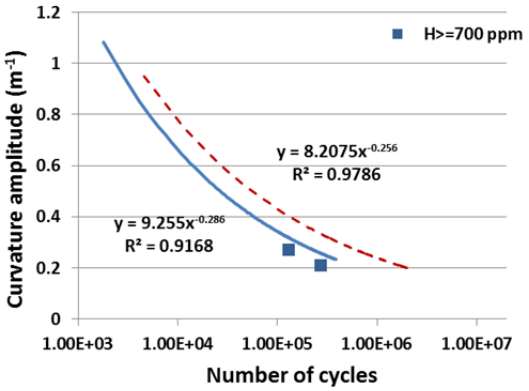


Fig.5. Curvature amplitudes as a function of number of cycles or κ-N curve for HBR used fuel with various levels of hydrogen content. The power function was obtained from curve fitting based on the HBR data set; the solid line corresponds to H >= 700ppm, and the dashed line corresponds to H < 700pm [5].

## III. CIRFT TESTING OF NORTH ANNA M5™ AND MOX M5™ UNF

### III.A. Static Testing of North Anna M5™ UNF

Three static CIRFT samples were tested in hot cell.

*III.A.1 NA3/651D3*

The static test was conducted on the specimen with the CIRFT label NA3 (fuel segment 651D3) under a displacement control mode using the following test procedure:

1. Ramp up to 12.00 mm at 0.1 mm/s rate at each loading point or each Bose motor.
2. Return to 0.0 mm at 0.2 mm/s.
3. If the rod specimen does not fail, repeat steps 1 and 2 four times.

Specimen NA3 survived four loading cycles without any sign of failure. The moment-curvature curves and equivalent stress-strain curves are shown in Fig. 6. In the estimates of equivalent stress and strain, the inside and outside diameters of 8.293 and 9.683 mm were used, respectively. There was a significant nonlinear deformation after 30 N·m; the maximum moment of 47 N·m was attained during the initial loading cycle. A deflection point appeared at approximately 8 N·m in the initial loading cycle. Subsequent loading cycles did not produce additional deformation, but they did introduce a closed hysteresis loop. The maximum curvature under a relative displacement of 24.00 mm at the loading points of the U-frame (i.e., 12.00 mm at each motor) was 4.1 $m^{-1}$. The maximum equivalent stress and strain obtained were 522 MPa and 2%, respectively. The rod appeared to be bent with significant plastic deformation after the static tests as shown in Fig. .

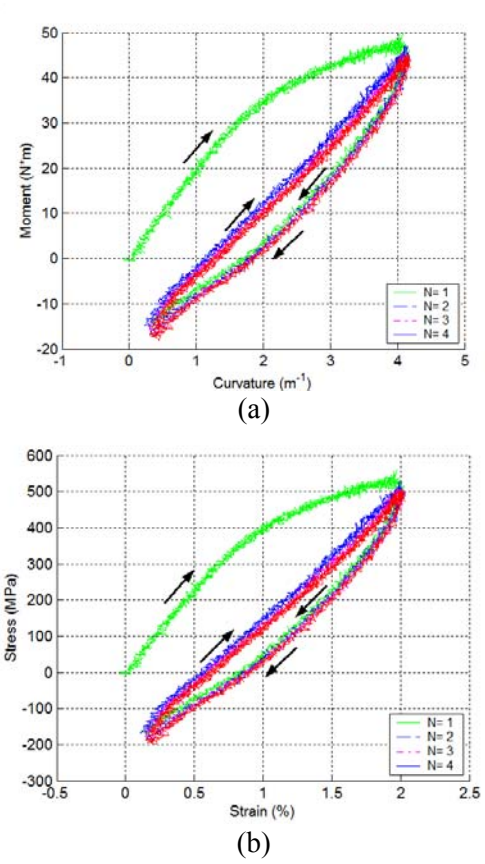


Fig. 6. (a) Moment-curvature curves and (b) equivalent stress-strain curves based on the first four loading cycles for specimen NA3 (651D3).

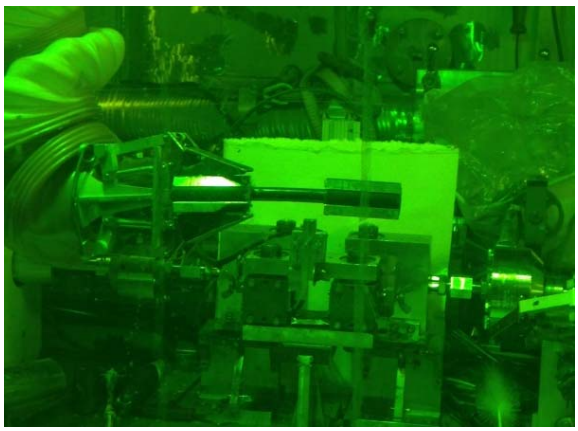

Fig. 7 Image of specimen NA3 (651D3) after testing; the rod sustained four cycles of loading to 24.00-mm relative displacement; the maximum moment with a level of 47 N·m was reached during the initial loading cycle.

### III.B. Dynamic Testing of North Anna M5$^{TM}$ UNF

Three dynamic tests were conducted in the hot cell. Applied moment amplitudes varied from ±7.62 to ±12.70 N·m. The fatigue life ranged from $1.57 \times 10^4$ to $6.1 \times 10^4$ cycles. The results of specimen NA2 are described below.

*III.B.1. NA2/651C5 under 10.16 N·m 5Hz*

The test on NA2 (651C5) was conducted under ±10.16 N·m, 5 Hz. A fatigue life of $2.2 \times 10^4$ cycles was obtained. Periodic quasistatic measurements of rod deformation were conducted using two relative displacement levels—1.0 and 2.0 mm—at the target intervals as described in Ref 11. Variations of the curvature, moment, and flexural rigidity as a function of number of cycles are given in Fig.8. The flexural rigidity of the rod stayed between 22 and 25 Nm$^2$ during most of the cycle testing period. This value of rigidity is a little lower than but still close to that of NA2. The results from online monitoring are given in Fig., and the image showing the failure location of the rod specimen as well as fractured surface profile is given in Fig..

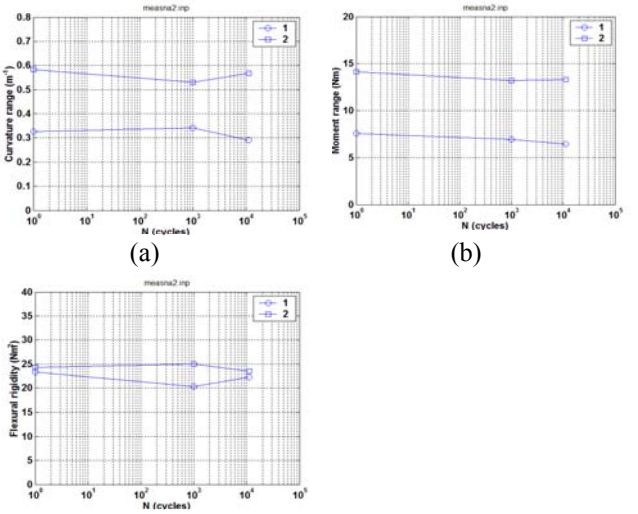


(a) (b) (c)

Fig. 8. Variations of (a) curvature range, (b) moment range, and (c) flexural rigidity as a function of number of cycles for NA2 (651C5). Measurements were made with 1.0 and 2.0 mm relative displacements; $N_f = 2.2 \times 10^4$ cycles under ±10.16 N·m, 5 Hz.

### III.C. Dynamic Testing of MOX UNF

Four static CIRFT samples were tested in hot cell. Applied moment amplitudes varied from ±5.08 to ±10.16 N·m. The fatigue life ranged from $3.7 \times 10^4$ to $2.1 \times 10^6$ cycles. The results of specimen MOX2 are described below.

*III.C.1 MOX2/ MOX-A-12 under 10.16N·m 5Hz*

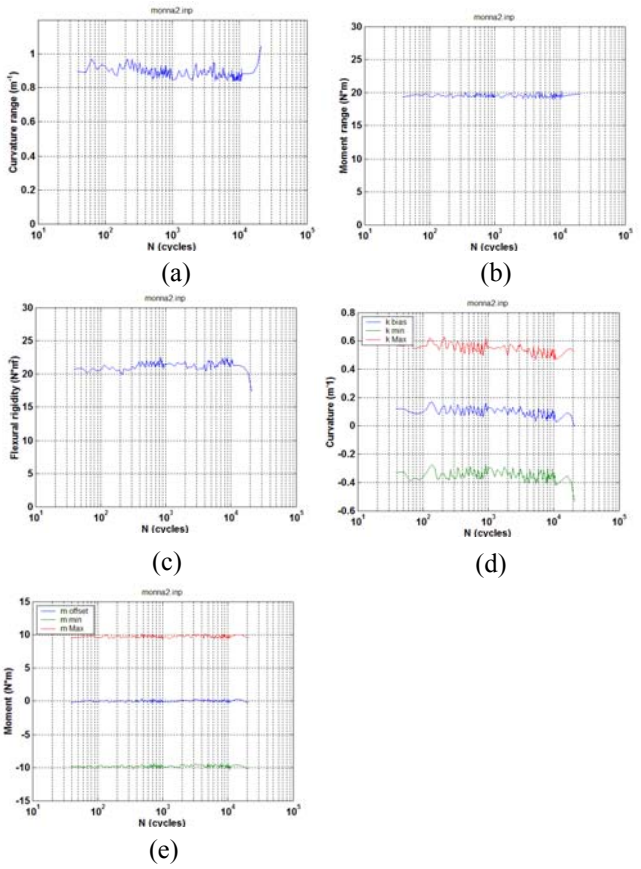


(a) (b) (c) (d) (e)

Fig. 9. Variations of (a) curvature range, (b) applied moment range, (c) flexural rigidity, (d) maximum and minimum values of curvature, and (e) maximum and minimum values of moment as a function of number of cycles for NA2 (651C5); $N_f = 2.2 \times 10^4$ cycles under ±10.16 N·m, 5 Hz.

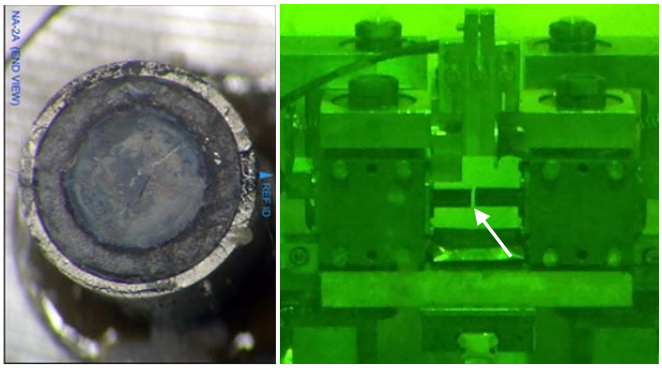

Fig. 10. Failure cross-section and fracture location of NA2 (651C5), $N_f = 2.2 \times 10^4$ cycles under ±10.16 N·m.

The test on MOX2/MOX-A-12 was conducted under ±10.16 N·m, 5 Hz. A fatigue life of $3.70 \times 10^4$ cycles was obtained. Periodic quasistatic measurements of rod deformation were conducted using two relative displacement levels—0.8 and 1.6 mm—at the selected

target number of cycles as described above. Time history of moment and curvature and curvature-moment loops obtained at the first cycle and 11,000 cycles are shown in Fig. 11. The curvature range–moment range and flexural rigidity are illustrated in Fig. 12. The variations of these quantities as a function of number of cycles are given inFig. 13. The rigidity of the measurements showed a clear decreasing trend starting with 24 $Nm^2$ and then dropping to 20 $Nm^2$ at $1.1 \times 10^4$ cycles.

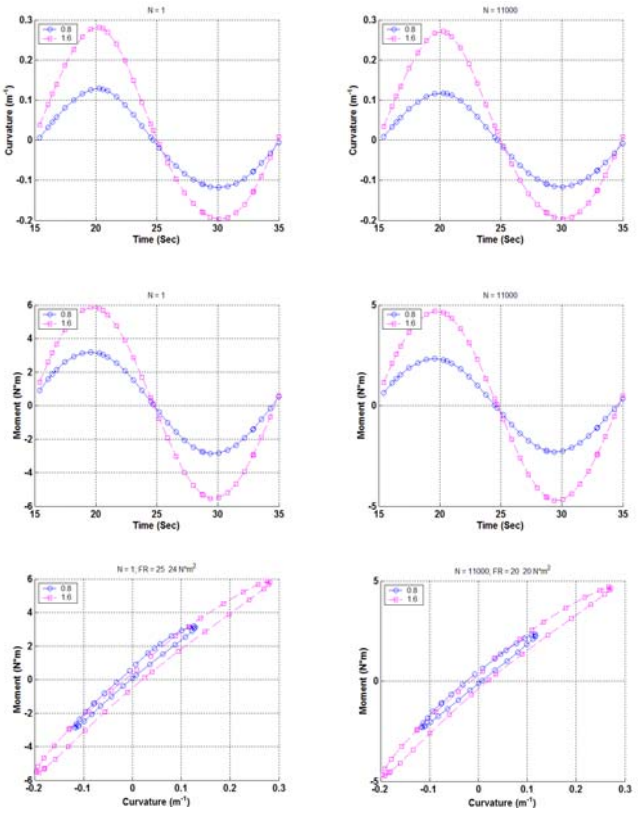


(a) (b)

Fig.11. Moment and curvature as a function of time and moment-curvature loops based on measurements when (a) N=1 and (b) N = 111,000 cycles for MOX2 (MOX-A-12). Measurements were made with 0.8 and 1.6 mm relative displacements; $N_f = 3.7 \times 10^4$ cycles under ±10.16 N·m, 5 Hz.

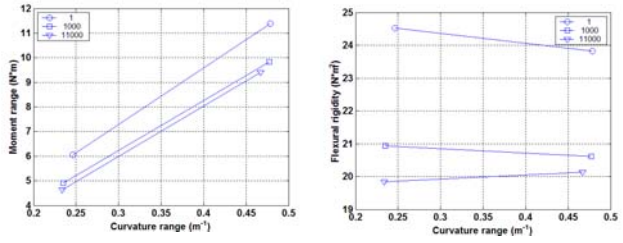


(a) (b)

Fig. 12. (a) Moment-curvature relation and (b) moment-flexural-rigidity relation at various numbers of cycles for MOX (MOX-A-12). Measurements were made with 0.8 and 1.6 mm relative displacements; $N_f = 3.7 \times 10^4$ cycles under ±10.16 N·m. 5 Hz.

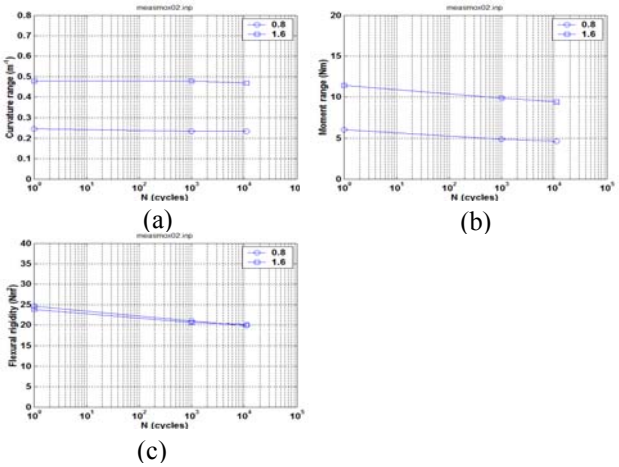


(a) (b)

(c)

Fig. 13. Variations of (a) curvature range, (b) moment range, and (c) flexural rigidity as a function of number of cycles for MOX (MOX-A-12). Measurements were made with 0.8 and 1.6 mm relative displacements; $N_f = 3.7 \times 10^4$ cycles under ±10.16 N·m, 5 Hz.

The curvature range, moment range, and flexural rigidity based on online monitoring data are presented in Fig.4, along with the maxima and minima. Online monitoring showed that flexural rigidity was essentially stable with a small amount of decrease (19 to 18 $Nm^2$) prior to the failure. The degree of decrease is lower than the value seen in the measurement. At the same time, the positive offset of curvature with an initial level of 0.1 $m^{-1}$ tended to become smaller during the cycle test.

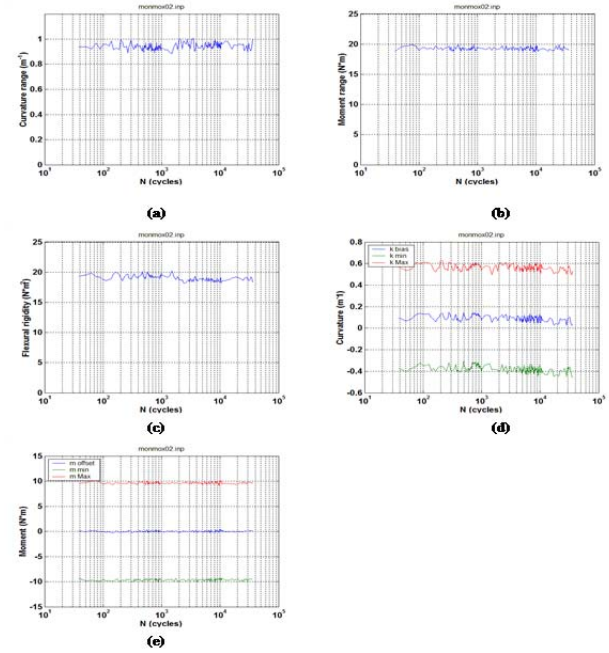


Fig. 14. Variations of (a) curvature range, (b) applied moment range, (c) flexural rigidity, (d) maximum and minimum values of curvature, and (e) maximum and minimum values of moment as a function of number of cycles for MOX2 (MOX-A-12).

## IV. CIRFT TEST RESULTS DISCUSSION

A summary of dynamic testing results for all of the UNF rods is represented in Fig. in terms of equivalent strain amplitude. Under the same level of amplitudes, the NA and MOX fuels showed a shorter fatigue life than HBR fuel. The difference between NA/MOX and HBR fuel is several tens of thousands of cycles. These data correspond with the lower yielding of NA/MOX fuels c. However, the fatigue mechanism remains to be investigated. The alternate form is also given in Fig. in terms of maximum of absolute strain extremes. It is noted here that MOX4 and MOX6 CIRFT specimens both were tested under same loading condition of 5.08N-m. Twice two-foot drops were applied to MOX6 specimen before cyclic fatigue testing; Fig. 15 shows a slightly increase in strain amplitude for MOX6 specimen (likely due to impact induced stiffness degradation) compared to that of MOX4 specimen, however, MOX6 fatigue life is significant less than that of MOX4 specimen.

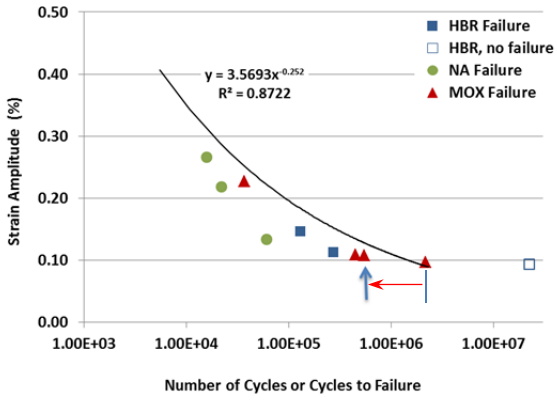


Fig. 15. Strain amplitudes as a function of number of cycles; results are based on CIRFT testing at 5 Hz. The power function was obtained from curve fitting based on the HBR data set [5]. The data point with the arrow represents two-foot drop test applied to CIRFT specimen before the dynamic vibration test being carried out.

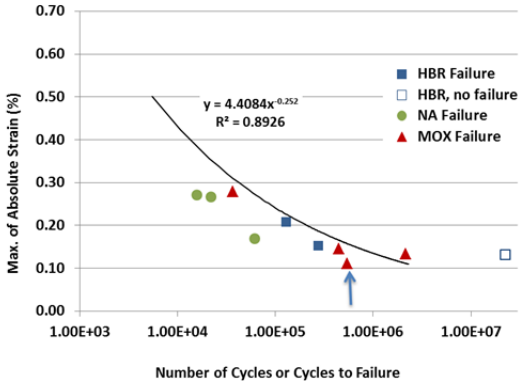


Fig. 16. Maxima of absolute strain extremes as a function of number of cycles; results are based on CIRFT testing at 5 Hz. The power function was obtained from curve fitting based on the HBR data set [5]. The data point with the arrow represents the two foot drop test of the specimen.

## V. FINITE ELEMENT ANALYSIS OF M5™ CLAD MATERIAL

The finite element analysis (FEA) model of an M5™ fuel rod system is formed by $UO_2$ pellets and M5™ cladding [Ref. 2]. It incorporates appropriate boundary conditions including the bonding layer at clad/pellet interfaces. The model consists of a fuel rod with a 3-dimensional (3D) representation of fuel pellets, clad, and possible combinations of gaps at the pellet-pellet and pellet-clad interfaces. The ABAQUS code was used, and the fuel rod was represented by a beam element with the associated effective stiffness. This approach was used to obtain the effective properties of the beam elements for use as input for further development of the detailed UNF assembly model. The approach is also designed to estimate the damping properties of the beam elements due to frictional resistance between the clad and the embedded pellets. This pellet-clad interaction modeling uses a "contact element" algorithm and can be further implemented into other embedded boundary conditions such as internal pressure and residual stress.

The FEA simulation results were also calibrated and benchmarked with CIRFT fatigue aging data [Ref. 5]. Based on FEA simulation results, the impacts of interfacial bonding efficiency at pellet-pellet and pellet-clad interfaces on the M5™ fuel rod performance can be summarized as follows [Ref. 9-10]. With good interface bonding and without fuel pellet and clad fracturing, the pellets in the fuel rod will carry more bending moment resistance than the clad under NCT vibration. The maximum stress resides in the pellets, and the stresses at the clad and pellet are both below the yield condition. Therefore, the system is in a linear elastic state under the target bending loads. There is no shear stress surge inside the M5™ cladding.

Upon fuel pellet failure, including debonding at the pellet-pellet interfaces, the load-carrying capacity shifts from the fuel pellets to the clad. The clad starts to carry most of the bending moment at the pellet-pellet interface region, resulting in localized stress concentrations in the clad. However, under the target bending moment, the clad does not yield. With good cohesion bonding at the pellet-clad interfaces, the pellets can continue to support the clad and carry a sufficient portion of the bending moment resistance. Therefore, most of the clad at the gauge section remains in the linear elastic range. A shear stress surge occurs inside the cladding at the pellet-pellet interface regions.

When further debonding occurs at the pellet-clad interfaces, the embedded pellets can no longer provide effective structural support to the clad; nor can they assist load transfer within the fuel rod system. Thus most of the

load-carrying capacity shifts to the clad throughout the entire gauge section. The shift leads to uniform maximum stress in the clad in the entire gauge section instead of at localized pellet-pellet interface regions due to stress concentrations.

## VI. CONCLUSIONS

The CIRFT was conducted on three HBR rods (R3, R4, R5); two specimens failed and one specimen did not fail. The total number of cycles in the test of nonfailed specimens went over $2.23 \times 10^7$; the test was stopped because the specimen did not show any sign of failure. Data analysis demonstrated that it is necessary to characterize the fatigue life of UNF rods in terms of both the curvature amplitude and the maximum of absolute curvature extremes. The latter is significant because the maxima of extremes signify the maximum of tensile stress of the outer fiber of the bending rod. A large range of hydrogen content has been covered in CIRFT on HBR rods. The load amplitude has been the dominant factor that controls the fatigue life of rods, but the hydrogen content also has an important effect on the fatigue life, as illustrated in Fig. 5.

Seven dynamic tests at 5 Hz were conducted in the hot cell: three NA M5$^{TM}$ specimens and four MOX specimens. The moment amplitudes tested were 5.08–12.70 N·m, and the curvature amplitudes were 0.200–0.55 $m^{-1}$. The equivalent stress amplitudes were 59.12–142.37 MPa, and the equivalent strain amplitudes were 0.10–0.27 %. The fatigue life of the rods decreased from $2.15 \times 10^6$ to $1.57 \times 10^4$ cycles. It is noted here that the dynamic test also reveals the potential accelerated aging from the drop during handling or the transient shocks of NCT.

Based on a series of FEA simulations on M5$^{TM}$ clad, the impact of the interface bonding efficiency on UNF vibration integrity, the distribution of moment carrying capacity between pellets and clad, and the impact of the interface material on the flexural rigidity of the M5$^{TM}$ fuel rod system are all important factors to be considered when evaluating the clad/fuel system under NCT. The immediate consequences of interface debonding are a shift in load-carrying capacity from the fuel pellets to the clad and a reduction in composite rod system flexural rigidity. Therefore, the flexural rigidity of the fuel rod and the bending moment resistance capacity between the clad and fuel pellets are highly dependent on the interface bonding efficiency at the pellet-pellet and pellet-clad interfaces. Furthermore, the curvature and associated flexural rigidity estimates based on global measurement of CIRFT tests are very different from the localized clad data estimated by FEA. As a result of the lack of pellet support at the debonded interface, the local tensile clad curvature is ~3 to 4 times that of the global curvature at the tension side of the clad. And significant stress concentrations were observed in the pellet-pellet-clad tri-interface regions. The potential weakest link of a UNF system is resided at the pellet-pellet interface region, due to its stress concentration. Furthermore, from the UNF CIRFT testing, the fractured CIRFT specimens are almost all failed or initiated at pellet-pellet interface regions.

## ACKNOWLEDGMENTS

This research was sponsored by the DOE Used Fuel Disposition Campaign (UFDC) and NRC under DOE contract DE-AC05-00OR22725 with UT-Battelle, LLC. Authors thank Chuck Baldwin for PIE, Josh Schmidlin for fuel rod cutting and dimension measurement; Bryan Woody and Scot Thurman for hot-cell operation support.

## REFERENCES

1. H. Wang, J.-A. J. Wang et al., "Development of U-frame Bending System for Studying the Vibration Integrity of Spent Nuclear Fuel," *Journal of Nuclear Materials* 440, 201–13 (2013).
2. J-A. Wang, H. Wang, H. Jiang, B. Bevard, R. Howard, "CIRFT Testing Results on High Burnup UNF," *M2-FCRD-UFD-2014-000053*, September 2014.
3. J.-A. Wang, H. Wang, B. Bevard, M. Flanagan, et al., "Surrogate SNF Vibration Integrity Investigation," *2014 ANS Meeting*, June 15-19, 2014, Reno Nevada.
4. J.-A. J. Wang, H. Wang, et al., "Reversible Bending Fatigue Test System for Investigating Vibration Integrity of SNF During Transportation," *PATRAM 2013*, San Francisco, Calif., August 18–23, 2013.
5. J.-A. J. Wang and H. Wang, "Mechanical Fatigue Testing of High-Burnup Fuel for Transportation Applications," NUREG/CR, ORNL/TM-2014/214, Oak Ridge National Laboratory, December 2014.
6. J-A. Wang, H. Wang, B. Bevard, "Reversible Bending Fatigue Testing on Zry-4 Surrogate Rods," *WM2014 Conference*, Phoenix, AZ, March 02-06, 2014.
7. J.-A. J. Wang et al., *SNF T*est System for Bending Stiffness and Vibration Integrity, *International High-Level Radioactive Waste Management Conference*, Albuquerque, N.M., April 28–May 2, 2013.
8. J.-A. Wang, H. Wang, et al., "The Development of Reversible Bending Fatigue Tester and Its Application to High Burnup SNF Vibration Integrity Investigation under Normal Transportation," ORNL/TM-2013/573.
9. H. Jiang, J-A Wang, and H. Wang, "Potential Impact of Interfacial Bonding Efficiency on SNF Vibration Integrity during Normal Transportation," *ASME PVP Conference*, July 20-24, 2014, Anaheim CA.
10. J-A. Wang, H. Wang, and H. Jiang, "Using Finite Model Analysis and Out of Hot Cell Surrogate Rod Testing to Analyze High Burnup SNF Mechanical Properties," *FCRD-UFD-2014-000603,* August 2014.